Zeitschrift: Schweizerische mineralogische und petrographische Mitteilungen = Bulletin suisse de minéralogie et pétrographie

Band: 84 (2004)

Heft: 1-2: Geodynamics and Ore Deposit Evolution of the Alpine-Carpathian-Balkan-Dinaride Orogenic System

Artikel: The Ada Tepe deposit: a sediment-hosted, detachment fault-controlled, low-sulfidation gold deposit in the Eastern Rhodopes, SE Bulgaria

Autor: Marchev, Peter / Singer, Brad S. / Jelev, Danko

DOI: https://doi.org/10.5169/seals-63739

Schweizerische Mineralogische und Petrographische Mitteilungen 84, 59–78, 2004

The Ada Tepe deposit: a sediment-hosted, detachment fault-controlled, low-sulfidation gold deposit in the Eastern Rhodopes, SE Bulgaria

Peter Marchev[1], *Brad S. Singer*[2], *Danko Jelev*[3], *Sean Hasson*[3], *Robert Moritz*[4] and *Nikolay Bonev*[5]

Abstract

The Ada Tepe gold deposit, 230 km SE of Sofia, formed in the eastern part of the Rhodope Mountains that underwent extension and metamorphic core complex formation, followed by normal faulting, basin subsidence, and silicic to mafic magmatism during the Maastrichtian–Oligocene. The region comprises numerous volcanic-hosted epithermal and base-metal vein deposits spatially and temporally associated with the Oligocene magmatism. Ada Tepe is a typical low-sulfidation epithermal gold deposit, unusual in that it is older than adjacent magmatic-related deposits and is hosted in Maastrichtian–Paleocene sedimentary rocks above a detachment fault contact with underlying Paleozoic metamorphic rocks.

Gold mineralization is located in: (1) a massive, tabular ore body above the detachment fault; and (2) open space-filling ores along predominantly east–west oriented listric faults. The ores are zones of intensive silicification and brecciation synchronous with detachment faulting. Brittle deformation opened spaces in which bands of opaline silica and electrum, quartz, pyrite, massive and bladed carbonates were deposited. Mineralization is exclusively a Au system with Au/Ag ~3, trace As and no base metals. Alteration consists of quartz, adularia, chlorite, sericite, calcite, pyrite and clay minerals. Adularia and abundant bladed carbonates indicate boiling within the entire span of the deposit, whereas bands of opaline silica with dendritic gold suggest that silica and gold were transported as colloids. The physical setting of formation of the Ada Tepe deposit was very shallow and low temperature. The Sr and Pb isotope ratios of carbonates and pyrite reflect hydrothermal fluid signatures derived predominantly from the metamorphic rocks.

The age of mineralization and association with the detachment fault suggest that gold mineralization at Ada Tepe is more closely linked to the Kessebir metamorphic core complex rather than to local magmatism.

Keywords: detachment fault, sediment-hosted, low-sulfidation epithermal, Eastern Rhodopes, Bulgaria.

1. Introduction

The Rhodope metallogenic province (Stoyanov, 1979) comprises numerous volcanic-hosted epithermal (Madjarovo, Chala, Zvezdel, Losen, Perama Hill, Sappes) and base-metal vein (Madan, Luki, Popsko, Thermes) deposits hosted by metamorphic basement (Marchev et al., 2000). The spatial and temporal association of these deposits with Oligocene magmatic centers is documented by the radioisotopic dating of Singer and Marchev (2000), Marchev and Singer (2002), Rohrmeier et al. (2002) and Ovtcharova et al. (2003).

The Ada Tepe deposit is one of a newly discovered group of gold deposits in the Eastern Rhodopes. These share many features with the adularia class of epithermal deposits, but they are atypical in that they are hosted mostly in sedimentary rocks and do not show direct relationships to local magmatic activity. Three of them, including Ada Tepe, Rozino and Stremtsi (Fig. 1), are major targets for commercial exploration. Exploration carried out in the last 2 years shows that Ada Tepe is the major potential economic deposit in the region.

The Ada Tepe low-sulfidation epithermal gold deposit is located 4 km SE of Krumovgrad in the Eastern Rhodopes, 230 km SE of Sofia (Fig. 1). Balkan Minerals and Mining AD (BMM; owned by Dundee Precious Acquisitions Inc.) operates

[1] Geological Institute, Bulgarian Academy of Sciences, Acad. G. Bonchev St., 1113 Sofia, Bulgaria. <pmarchev@geology.bas.bg>
[2] Department of Geology and Geophysics, University of Wisconsin-Madison, 1215 West Dayton St., Madison, WI 53706, USA.
[3] Balkan Mineral and Mining AD, 24 Saedinenie St, Krumovgrad, Bulgaria.
[4] Section des Sciences de la Terre, Université de Genève, rue des Maraîchers 13, CH 1211 Genève, Switzerland.
[5] Department of Geology and Paleontology, Faculty of Geology and Geography, Sofia University "St. Kliment Ohridski", 15 Tzar Osvoboditel Bd., 1504 Sofia, Bulgaria.

0036-7699/04/0084/59

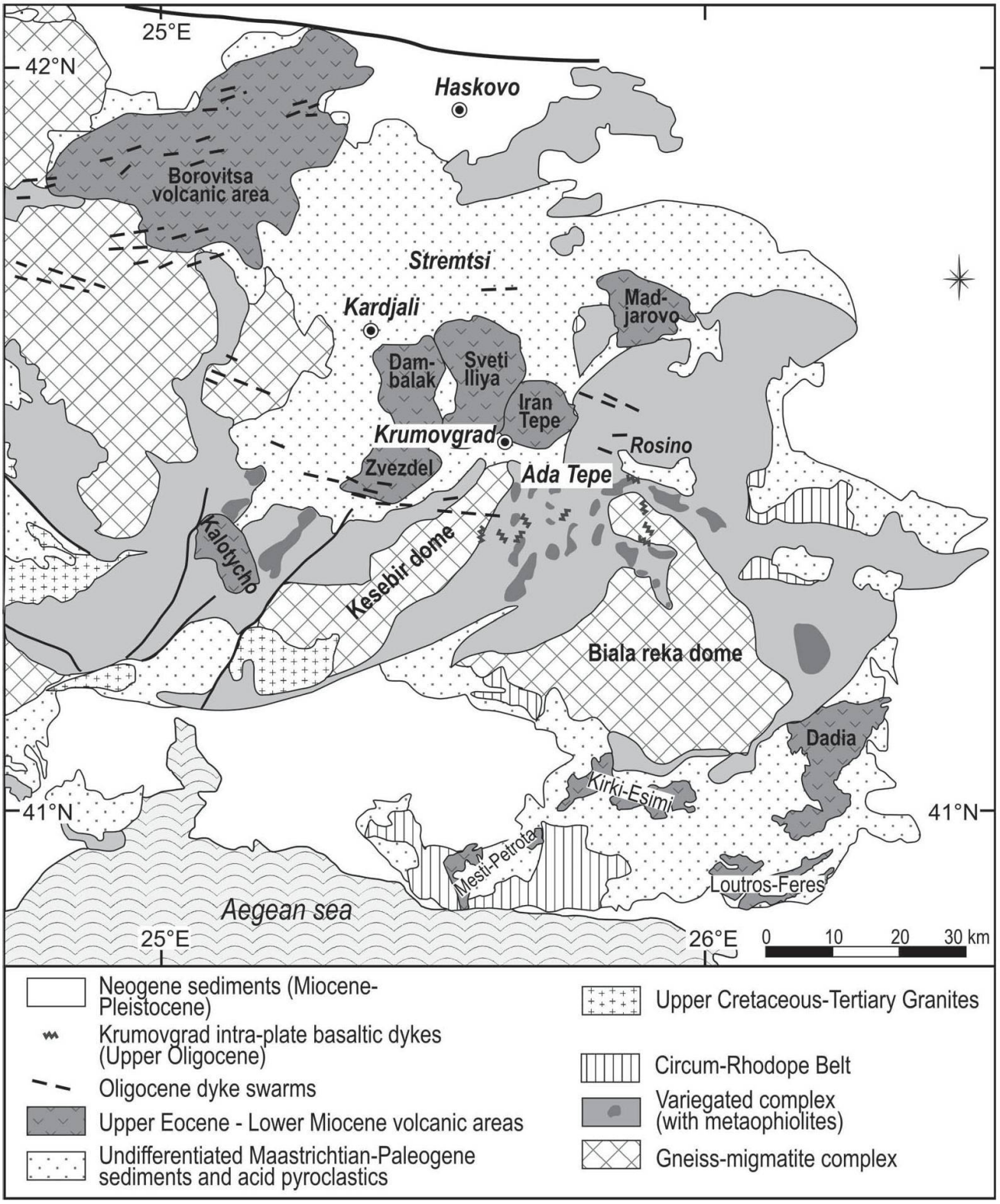

Fig. 1 Schematic geological map of the Eastern Rhodope showing metamorphic dome structures, major volcanic areas and dyke swarms. Compiled from Ricou et al. (1998), Yanev et al. (1998a) and Marchev et al. (2004). Inset shows location of Krumovgrad within Bulgaria.

this project. The deposit is unusual in that it is located along a regional detachment fault. Moreover, it is geochemically distinctive with respect to the adjacent deposits owing to high Au/Ag ratios and low base metal content (Marchev et al., 2003).

Here we summarize results from recent studies on the surface geology, structure, alteration types, and textural and mineralogical characteristics of the gold mineralization. The paper provides limited Sr and Pb isotope data for Ada Tepe and discusses the age relationships among gold mineralization, local igneous activity and thermal events in the nearby Kessebir metamorphic dome (Figs. 1, 2).

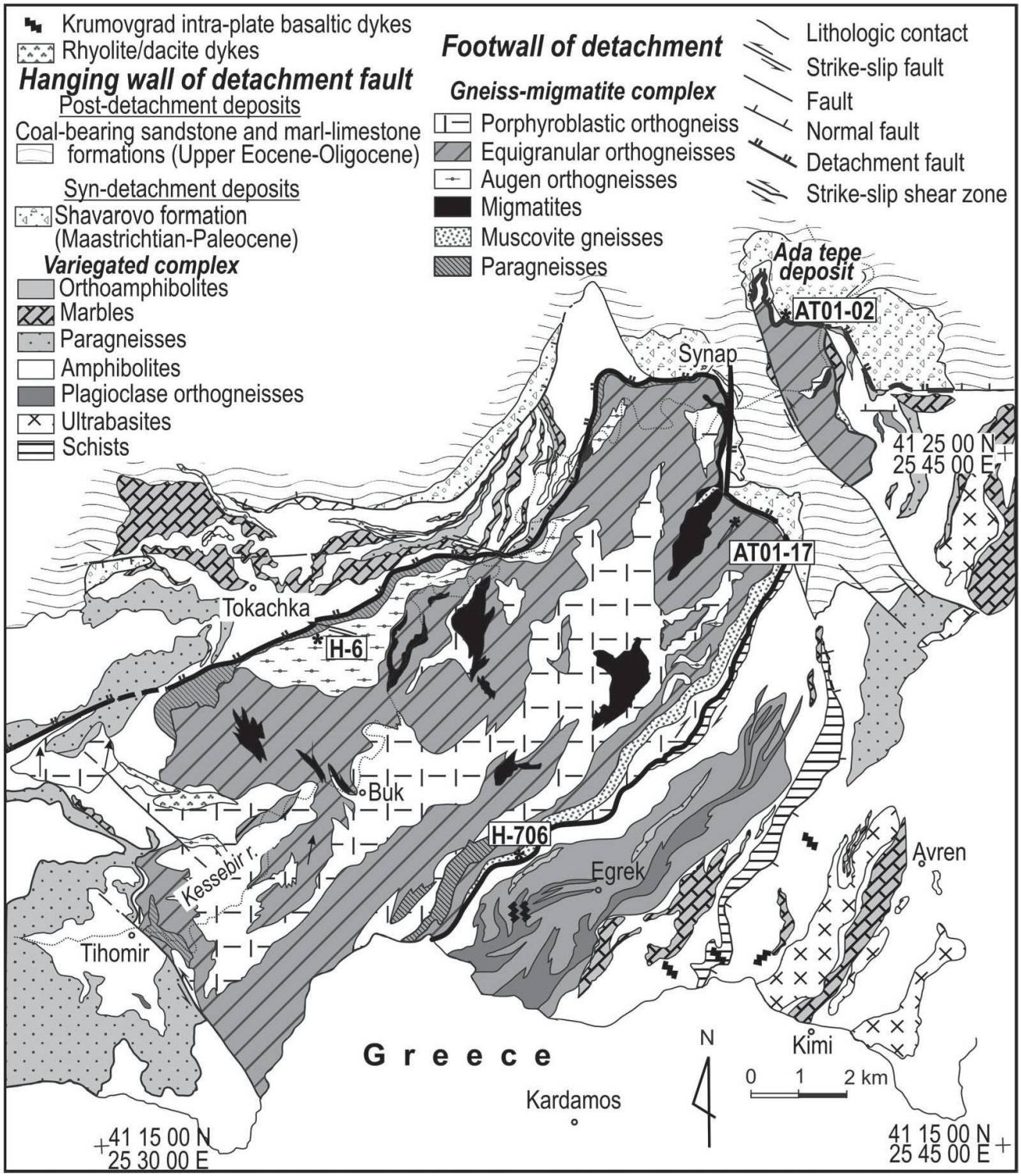

Fig. 2 Geological map of Kessebir dome (after Bonev, 2002) and location of Ada Tepe deposit and Synap prospect.

2. Historical background and previous studies

Small adits and large dumps at the eastern part of the Ada Tepe hill (Fig. 3a) provide tangible evidence for the historical mining activity, probably of Thracian and Roman times. Regional mapping of the Krumovgrad area was conducted in 1965 (Shabatov et al., 1965) and recently between 1995 and 1996 (Sarov et al., 1996) by the State exploration Company "Geology and Geophysics" at a 1:25 000 scale. Studies by Goranov and Atanassov (1992) and a Ph.D thesis by Bonev (2002) have clarified the stratigraphic and tectonic relationships of the Krumovgrad area. The latter work advocates a detachment-fault model for the formation of the Kessebir metamorphic dome. Limited exploration in the area of the Ada Tepe deposit was followed by the first description of its alteration and mineralization, and its classification as Au–Ag-polymetallic

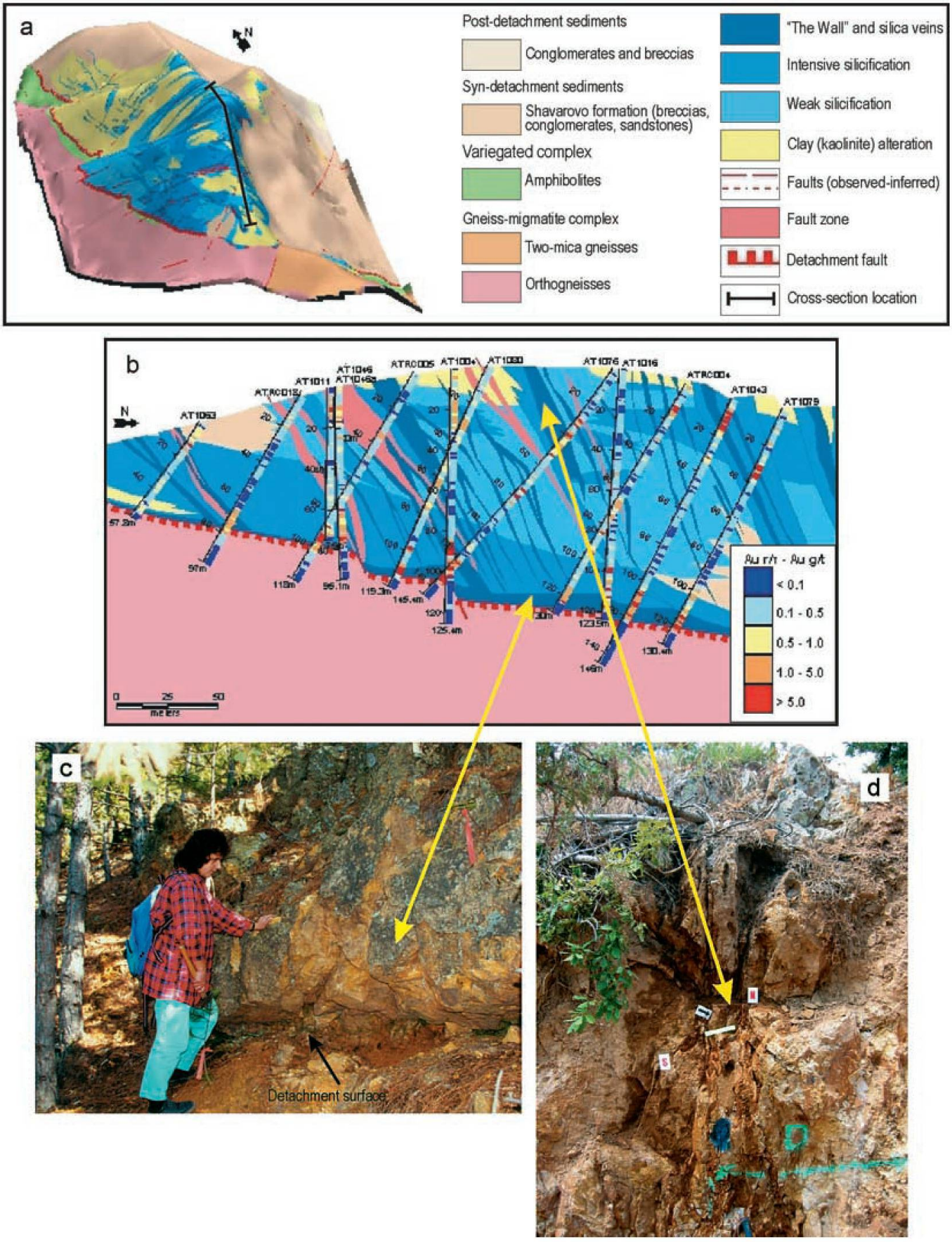

Fig. 3 (a) 3D view of Ada Tepe deposit. (b) Cross section of Ada Tepe deposit. Major ore bodies. (c) Massive, tabular ore body ("The Wall") above the detachment fault. (d) Open space-filling ores along predominantly E–W oriented listric faults.

occurrence of the adularia-sericite type (Kunov et al., 2001).

Since June 2000, the Ada Tepe deposit has been included in the Krumovgrad license area, and is explored by Balkan Mineral and Mining AD. Based on the results of regional mapping and surface sampling, BMM conducted two drilling programs, with 145 drill holes, using both diamond and reverse circulation drilling techniques, for a total length of 12 440 m. A total of 10 218 m of surface channel samples were also collected during 2001–2002. Resource calculations by RSG Global of Perth, Australia, show that Ada Tepe is a high-grade Au–Ag deposit containing 6.15 Mt of ore at 4.6 g/t Au for 910 000 ounces of Au, using a 1.0 g/t cutoff grade.

On the basis of initial results from the exploration program and the geographical proximity of the Ada Tepe deposit to the base metal mineralization at the Oligocene Zvezdel volcano, Crummy (2002) suggested a direct genetic link between the base and precious metal districts. Marchev et al. (2003) favoured an Upper Eocene age based on precise $^{40}Ar/^{39}Ar$ data and a detachment faulting model for the origin of the Ada Tepe deposit.

3. Geologic setting

3.1. District geology

Basement metamorphic rocks in the Krumovgrad area build up the elongated Kessebir dome in N–NE direction (Kozhoukharov et al., 1988; Ricou et al., 1998; Bonev, 2002) (Figs. 1, 2). Two major tectonostratigraphic units (complexes) have been recognized on the basis of composition and tectonic setting of the metamorphic rocks: a Gneiss-migmatite complex, and a Variegated Complex (Kozhoukharov et al., 1988; Haydoutov et al., 2001), which correspond to the Continental and Mixed units of Ricou et al. (1998), respectively. The structurally lower Gneiss-migmatite complex crops out in the core of the Kessebir metamorphic dome. It is dominated by igneous protoliths including metagranites, migmatites and migmatized gneisses overlain by a series of pelitic gneisses, and rare amphibolites. Eclogites and eclogitic amphibolites have been described in the Greek part of the Kessebir dome (Mposkos and Krohe, 2000). Rb–Sr ages of 334.6 ± 3.4 Ma (Mposkos and Wawrzenitz, 1995) from metapegmatites in Greece and Rb–Sr (328 ± 25 Ma) and U–Pb zircon ages of 310 ± 5.5 Ma and 319 ± 9 Ma (Peytcheva et al., 1995, 1998) from metagranites of the Kessebir dome in Bulgaria indicate that the Gneiss-migmatite complex is formed of Variscan or older continental basement.

The overlaying Variegated complex consists of a heterogeneous assemblage of pelitic schists, paragneisses, amphibolites, marbles and ophiolite bodies (Kozhoukharova, 1984; Kolcheva and Eskenazi, 1998). Metamorphosed ophiolitic peridotites and amphibolitized eclogites are intruded by gabbros, gabbronorites, plagiogranites and diorites. U–Pb zircon dating of a gabbro from the neighbouring Biala Reka dome (Fig. 1) yields a Late Neoproterozoic age of 572 ± 5 Ma for the core and outer zone recording a Hercynian metamorphic event at ~300–350 Ma (Carrigan et al., 2003). Volumetrically minor plutonic bodies of presumably Upper Cretaceous age intrude the Variegated complex, and represent an important phase of igneous activity in the area (Belmustakova et al., 1995). The rocks are medium to fine-grained, light grey, two-mica granites of massive to slightly foliated structure.

The rocks of the Variegated complex in the Krumovgrad area are overlain by the Maastrichtian–Paleocene syndetachment Shavarovo Formation (Goranov and Atanasov, 1992; see below), which is in turn overlain by Upper Eocene–Lower Oligocene coal-bearing-sandstone and marl-limestone formations. Lava flows and domes of the ~35 Ma andesites (Lilov et al., 1987) of the Iran Tepe volcano are exposed northeast of Krumovgrad (Fig. 1). This magmatic activity was followed by scarce dykes of latitic to rhyolitic composition in the northern part of the Kessebir dome, dated at 31.82 ± 0.20 Ma and finally by 26–28 Ma old intra-plate basaltic magmatism in the southern part of the dome (Marchev et al., 1997, 1998).

3.2. Deposit geology

The Ada Tepe deposit is hosted by the syndetachment Maastrichtian–Paleocene Shavarovo Formation, overlaying the northeastern closure of the Kessebir metamorphic core complex (Fig. 2). The contact between poorly consolidated sedimentary rocks and underlying metamorphic rocks corresponds to the location of a regionally developed low-angle normal fault, named the Tockachka detachment fault (TDF) by Bonev (1996). The fault dips 10–15° to the north-northeast. It can be traced further southwest for more than 40 km from Krumovgrad to the Bulgarian-Greek frontier and is well exposed in the area southwest of Synap village, about 2 km west of Ada Tepe. In the latter area, the rocks in the hanging wall of the TDF consist of metamorphic blocks, breccia, conglomerates, sandstone, marls and argillaceous limestone. This unit was first recognized by Atanasov and Goranov (1984) in the

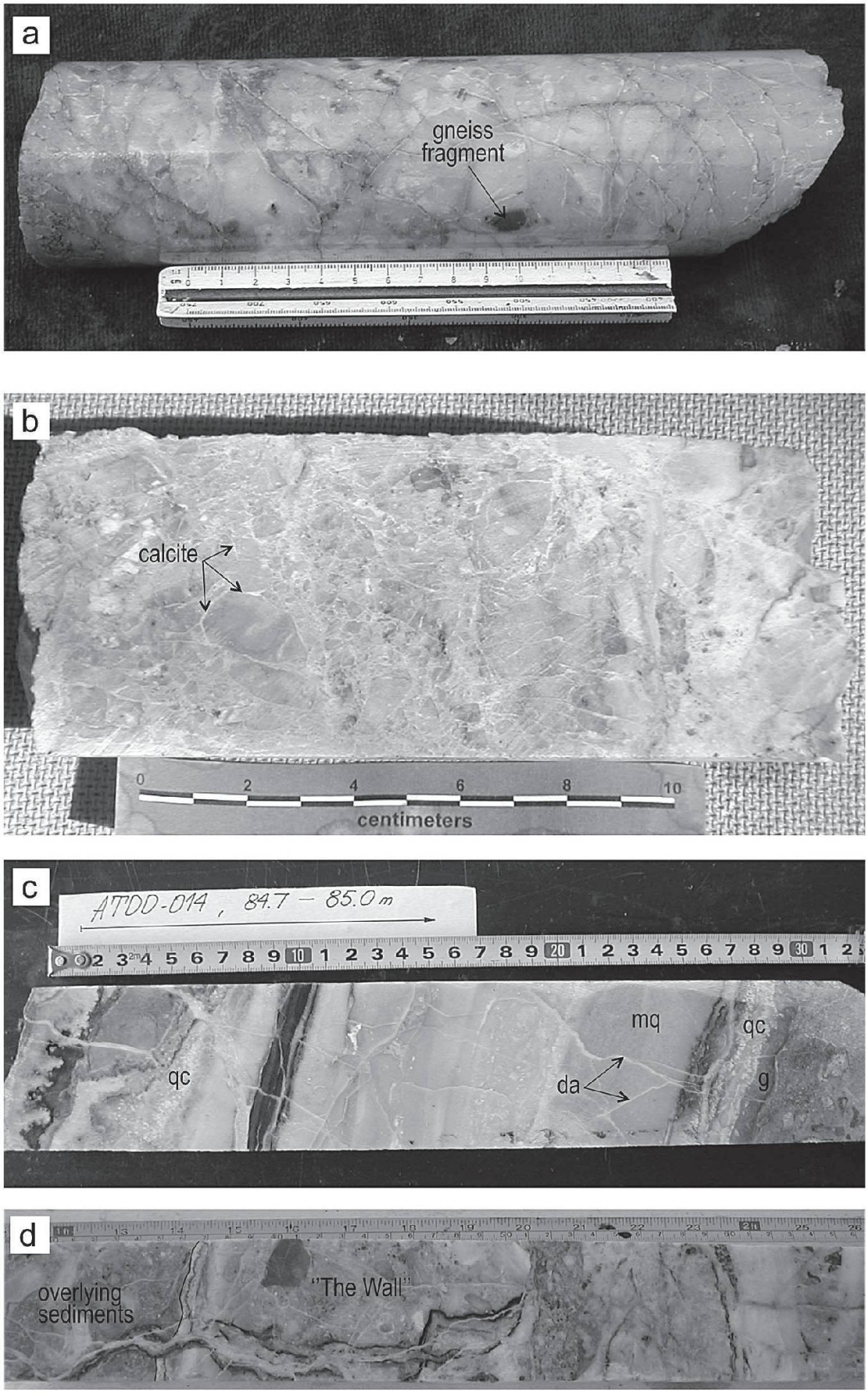

Fig. 4 Mineralization of The Wall showing multiple periods of silicification and veining. (a) Brecciated early microcrystalline silica (early stage) with a single gneiss fragment. (b) Breccia of the microcrystalline silica (early stage) cemented by calcite (third stage). (c) Subvertical colloform finely banded vein. Early stage gray (g) microcrystalline silica on the margins of the veins followed by the massive microcrystalline (mq) cross-cut by the third stage sugary quartz and massive and bladed calcite (qc). Late veinlets of dolomite-ankerite (da) cut early vein mineralization. (d) Transition of subhorizontal opaline carbonate vein into subvertical step-like vein in the overlying sediments.

Krumovgrad area and described as the Shavarovo Formation of the Krumovgrad Group in a later paper (Goranov and Atanasov, 1992). The total thickness of the type section of the Shavarovo Formation (~350 m) was measured along the Kaldjic river, near the Shavar village. Blocks and clasts of breccia and conglomerate are mixtures of gneiss, amphibolite and marble, derived primarily from the Variegated complex.

4. Structure

The dominant structure in the Ada Tepe prospect is the TDF. It is a mapable tectonic contact, best expressed along the western slope of Ada Tepe hill (Fig. 3a). In outcrop and drill cores, the fault is recognized as a contact between Paleozoic metamorphic rocks and Maastrichtian–Paleocene sedimentary rocks of the Shavarovo Formation. Immediately above the detachment fault there is a 0.5 to 20 m thick zone of massive silicification. In drill core, the lower limit of the structure is marked by a 10–20 cm-thick layer of tectonic clay. Gneiss, migmatite, marble and the amphibolite of the metamorphic basement beneath the detachment surface are transformed into a cataclastic rock over a thickness of several meters. The southwestern slope of the Ada Tepe hill is cut by a NW–SE-oriented high-angle fault (Fig. 2), which formed a small half graben fill by older Maastrichtian–Paleocene syndetachment sedimentary rocks overlain in the eastern part by younger Priabonian–Oligocene sedimentary rocks.

Major structures cutting the basement rocks of the Ada Tepe deposit are rare, although several E–W and N–S-oriented subvertical faults, marked by a zone of silicification, occur to the south, east and west of the Ada Tepe deposit. The longest N–S-striking zone has been traced for almost 200 m. The E–W and N–S faults coincide with the major directions of the mineralized veins in the sedimentary cover and can be interpreted as feeder structures for the mineralizing fluids.

5. Mineralization

5.1. Ore geometry and ore bodies

The Ada Tepe deposit is 600 m along strike and 300–350 m wide. Gold mineralization occurs as: (1) a massive, tabular body located immediately above the detachment fault (Figs. 3b, c), and (2) open space-filling within the breccia-conglomerate and sandstone along predominantly east-west oriented subvertical listric faults within the hanging wall (Figs. 3b, d). In cross section the tabular body dips (10–15°) to the north-northeast, which is consistent with the low angle TDF. The ore body is so strongly silicified; company geologists refer to it as "The Wall". Detailed observations on The Wall indicate a complicated sequence of events with multiple periods of silicification and veining. Silicification began with the deposition of massive white to light grey silica above the detachment fault partly or totally replacing the original rocks. Original rock textures were destroyed with the exception of ghosted gneiss fragments (Fig. 4a). The latter are rounded with veins of quartz or carbonate cutting or surrounding the clasts. Early microcrystalline silica was commonly veined by subvertical banded veins or brecciated by later fault movements and cemented by calcite, sugary quartz (Fig. 5b) or by pyrite.

In the less silicified parts The Wall consists of numerous differently oriented veins ranging in width from less than 1 cm up to 30 cm (Fig. 4c). Subvertical veins, which were formed by deposition of colloform silica layers in open space, can be traced from The Wall into the listric faults in the overlying sedimentary rocks (Fig. 4d). On the surface they form E–W-trending ridges, separated by argillic zones (Figs. 3a, b, d).

5.2. Ore and gangue mineralogy and stages of mineralization

The ore mineralogy of the Ada Tepe deposit is simple, consisting mainly of electrum and subordinate pyrite with traces of galena, and gold-silver tellurides. Gangue minerals consist of silica polymorphs (microcrystalline, fine-grained, sugary quartz and opaline silica), various carbonates (calcite, dolomite, ankerite and siderite), and adularia. Tellurides include hessite (Ag_2Te) and petzite (Ag_3AuTe_2). All samples with Au content higher than 1 g/t have almost constant Au/Ag ratios ~ 3, reflecting the composition of electrum (76–73 wt% Au).

Unlike the massive silicification of The Wall, banded veins in and above it provide an excellent framework for identifying the different stages of mineralization. Mineralization in Ada Tepe can be subdivided into 4 broad, generally overlapping stages of quartz and carbonate veins on the basis of cross-cutting relationships, changes in mineralogy, texture and gold grades.

The earliest stage is characterized by deposition of microcrystalline to fine-grained grayish to white massive or banded quartz with rare pyrite and adularia (Figs. 5a–d). In some veins silica deposition starts with a thin band of almost isotropic opaline (Fig. 4 c) followed by thin band of quartz with rare bladed calcite. Breccia texture is typical

for the massive silicification of The Wall. The products of the early stage form microfracture filling in the host rocks near the margins of the veins or rock fragments in The Wall, causing the silica-adularia-pyrite replacement in them. The gold grade of this stage is unknown.

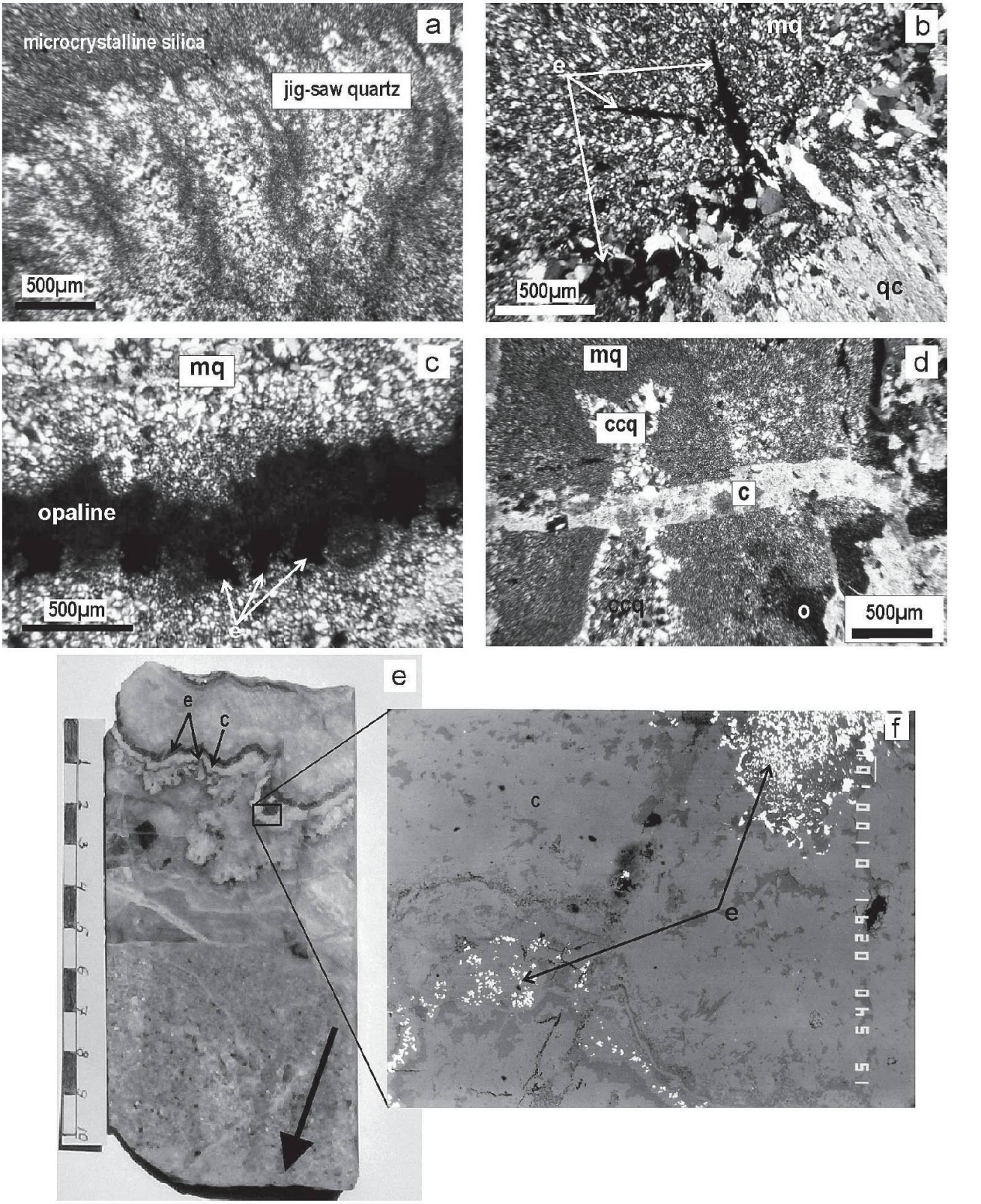

Fig. 5 Microphotographs and SEM images of silica and bonanza ore textures. (a) Bands of early stage microcrystalline (mq) and jigsaw quartz (jq). (b) Electrum band (e) deposited on the interface between early microcrystalline quartz (mq) and third stage sugary quartz and radiating bladed calcite (qc). (c) Band of electrum (e) and isotropic opaline. Electrum is located on the bottom of the band. (d) Third stage coarse crystalline quartz (ccq), cutting the opaline (o) and microcrystalline quartz (mq), which in turn is cut by calcite (c). (e) Subparallel bands of electrum (e) and microcrystalline adularia and silica separated by a calcite vein (c). The arrow shows the vertical direction. (f) SEM image of the outlined area.

The economic gold is related to the second stage of mineralization. It starts at the end of the microcrystalline quartz and the beginning of the coarser grained (sugary) quartz of the third stage below (Fig. 5b). Usually, it forms black millimeter-scale bands of opaline or microcrystalline chalcedony-adularia and electrum (Figs. 5c–f). Locally opaline silica crosscuts the microcrystalline quartz (Figs. 5c–d) of the early stage and in turn is cut by the coarser grained quartz and carbonates of the third and forth stages (Figs. 5d–e). Petrographic examination of the electrum-rich bands reveals that electrum commonly occurs towards the bottom of the opaline or microcrystalline bands (Figs. 5c, e). Where opaline bands are not present, electrum precipitates at the boundary of first and third stages (Fig. 5b). The electrum has irregular forms as the result of crystallization in the quartz interstices, being relatively well-shaped in the coarser-grained quartz crystals. The size of electrum grains ranges from less than 1 to 20 μm. However the single crystals form chains reaching up to 650 μm (Figs. 5b, 6a). Electrum in gold-rich bands etched with HF is characterized by botryoidal surfaces that appear to have formed by the aggregation of spherical electrum particles (Figs. 6a–b), as observed in the Sleeper deposit, Nevada (Saunders, 1990, 1994). Electrum in bonanza veins can occupy 50 vol% (Figs. 5f, 6c), accompanied by rare As-bearing pyrite. Occasionally, micron or submicron size electrum inclusions form zones within the As-bearing pyrite (Figs. 6d). Tiny Au–Ag tellurides have been observed at the contacts between electrum grains and small galena crystals (Fig. 6f).

The third stage starts with deposition of sugary quartz (up to 1.5 mm large; Figs. 5d, 7a) followed by bands of quartz and bladed calcite (Figs. 5b, 7b) and finally by massive calcite with small amount of quartz (Fig. 5d). Locally, calcite fills quartz geodes or forms small veins (Fig. 7a). Microscopically the late calcite corrodes and replaces quartz crystals. Small amount of adularia and pyrite are also typical for this stage.

The hydrothermal mineralization ended with the deposition of pinkish ankerite-dolomite and siderite, which was preceded by precipitation of massive pyrite in some parts of the deposit (Figs. 7c–d).

The mineralization of Ada Tepe exhibits several important spatial and textural features that provide insights to the physical environment of ore deposition. In its upper part, quartz becomes the predominant gangue mineral, whereas carbonates are subordinate. This is particularly obvious in the last stage, where in the surface samples dolomite and ankerite are absent in the geodes and bladed minerals consist of microcrystalline quartz only. Another spatial variation is the diminishing of banding textures with the decrease in grade of Au mineralization to the north. An important feature is the absence of bladed carbonates in the veinlets beneath The Wall, in contrast to the entire extent of the deposit above the detachment surface.

5.3. Oxidized zone

The uppermost part of the Ada Tepe deposit has been oxidized by supergene processes with the depth of oxidation being dependent upon intensity of faulting. Due to extensive silicification, The Wall itself is generally not oxidized; however, a 2 to 5 m thick zone of oxidation invariably occurs above The Wall. Narrow zones of oxidation occur down to this zone utilizing high angle listric faults. These faults and fractures most likely acted as conduits for the surface waters to reach the impermeable silicified zone, forming the oxidized zone above The Wall.

Most of the pyrite in the oxidized zones has been converted into limonite identified as goethite. Kaolinite is widely distributed in this zone, forming locally small veinlets. Electrum in the oxidized zone however, shows no evidence of Au enrichment.

6. Alteration

In the poorly mineralized zones hydrothermal alteration is weak with most of the detrital minerals (quartz, muscovite and feldspars) remaining unaltered. Alteration consists of chlorite, calcite, kaolinite and subordinate albite, pyrite and ankerite-dolomite. It seems that calcite and ankerite-dolomite are late; however, it is difficult to distinguish replacement calcite from vein calcite. Quartz, adularia, calcite, pyrite and dolomite-ankerite-siderite ± sericite and clay minerals in variable proportions occur in The Wall and immediate proximity to the subvertical quartz and carbonate veins in the strongly mineralized zones. They formed through replacement of the original metamorphic minerals included in the sandstone and conglomerate, and are associated with relict, detrital quartz and muscovite. This complex mineral assemblage is the result of the evolution of the hydrothermal activity.

Hydrothermal alteration of the basement metamorphic rocks is developed within a halo several meters in extent beneath The Wall, and is more pronounced around the subvertical veins. The alteration assemblage includes quartz, adu-

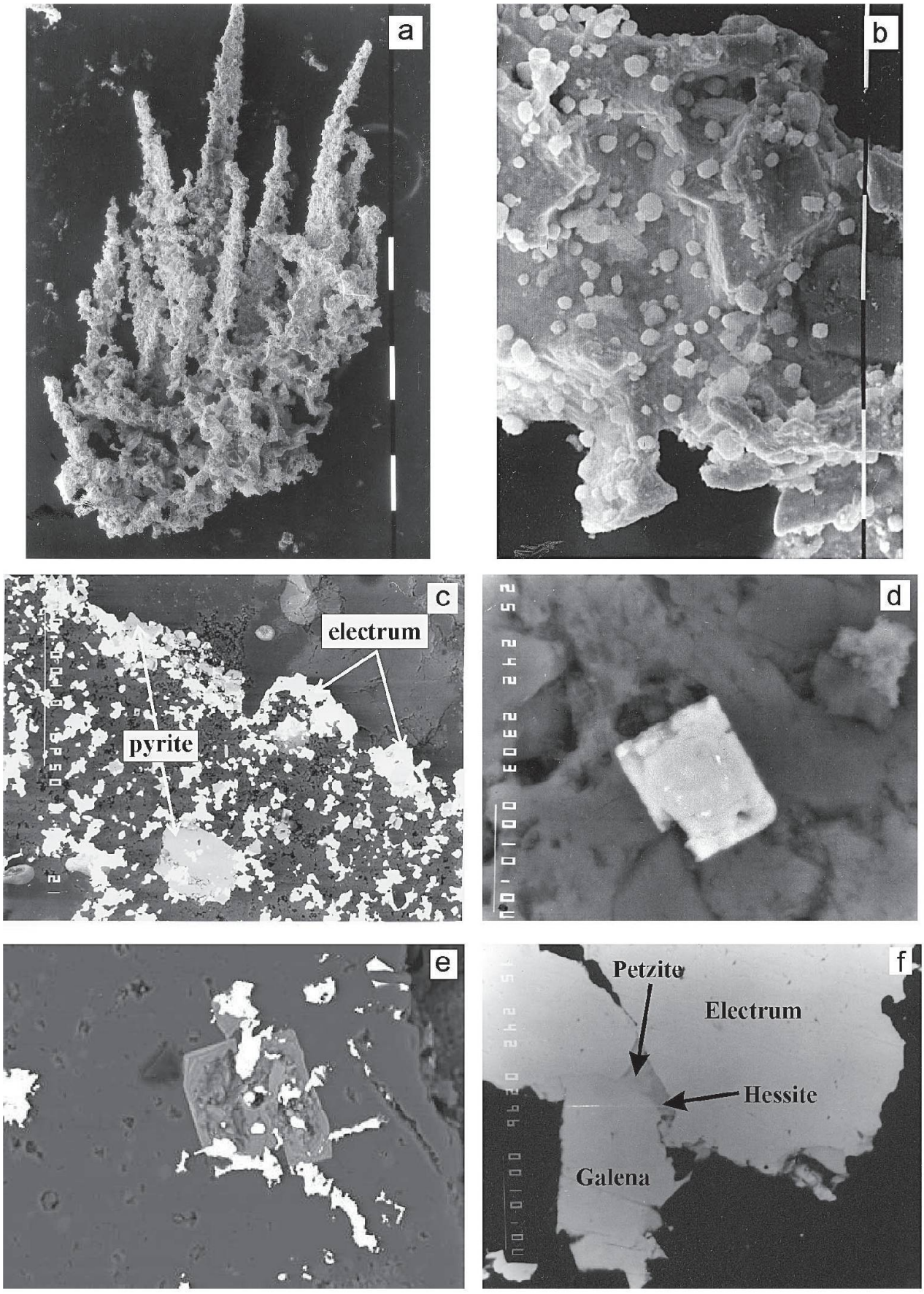

Fig. 6 (a) SEM images of electrum dendrite etched with HF. (b) Negative forms of quartz removed by HF and spherical colloidal particles. (c) Opal-electrum band, containing ~ 50% electrum and small amount of pyrite. Dark crystals between electrum are adularia and silica; (d) Pyrite with a zone of submicron-size electrum; (e) Former Py converted to goethite with inclusions of Au. (f) Au–Ag tellurides between larger electrum and galena crystals.

laria, illite or sericite, pyrite, kaolinite, and late stage ankerite-dolomite-siderite.

Clay minerals are more abundant and better developed in the alteration close to the surface where they form argillic zones between the E–W-oriented swarms of veins. Kaolinite and quartz predominate in the argillic zones, and illite, chlorite, adularia and carbonate are subordinate, accompanied locally by illite-montmorillonite. Part of the shallow-level kaolinite may be supergene, but its association with unoxidized pyrite beneath and within The Wall indicates that a hypogene origin is likely at least for the deeper kaolinite.

7. Geochronology

$^{40}Ar/^{39}Ar$ ages from adularia and sanidine samples were determined to constrain the timing of mineralization and volcanic activity in the Kessebir dome. Sample AT01-2, from which adularia was extracted for dating, is from a drill-hole at 72.5 m depth. It represents a quartz-adularia-carbonate banded vein filled with finely veined gneiss clasts. It is a mixture of completely replaced detrital K-feldspar and directly deposited adularia crystals. The rhyolite dyke (sample AT01-17) is emplaced within the core orthogneisses of the Kessebir dome located 4 km southwest from Ada Tepe (Fig. 2). It comprises 2 cm diameter sanidine phenocrysts that were separated for dating, plus plagioclase, biotite, and quartz.

$^{40}Ar/^{39}Ar$ experiments were conducted at UW-Madison Rare Gas Geochronology Laboratory. Minerals were separated from 100–250 micron sieve fractions using standard magnetic, density, and handpicking methods. Five milligrams of each mineral were irradiated at Oregon State University, U.S.A. for 12 hours, along with 28.34 Ma sanidine from the Taylor Creek rhyolite as the neutron fluence monitor. Analytical procedures, including mass spectrometry, procedural blanks, reactor corrections, and estimation of uncertainties are given in Singer and Brown (2002). Isotopic measurements were made of the gas extracted by incrementally heating of 2–3 mg multi-crystal aliquots using a defocused CO_2 laser beam. Results of incremental heating experiments along with the $^{40}Ar/^{39}Ar$ ages of muscovite and biotite from the lower plate of the metamorphic basement rocks taken from Bonev et al. (accepted) are in Table 1. Incremental heating experiments and age spectra of the sanidine and adularia are presented in Table 2 and Fig. 8. Uncertainties in the ages include analytical contributions only at $\pm 2\sigma$.

The plateau age of the adularia, based on 79.3% of the gas released, is 34.99 ± 0.23 Ma (Fig. 8) and is indistinguishable from the total fusion age of 35.05 ± 0.23 Ma. Sanidine from the rhyolite dyke yielded a plateau age of 31.82 ± 0.20 Ma based on 60 percent of the gas released, which is indistinguishable from the total fusion age of 31.88 ± 0.20 Ma. As is the case for the adularia, this indicates that argon loss due to weathering or alteration is negligible. Moreover, the inverse isochron ages of 35.11 ± 0.37 Ma for the adularaia and 31.91 ± 0.27 Ma for the sanidine are indistinguishable from the plateau ages and the $^{40}Ar/^{36}Ar$ intercept values indicate that there is virtually no excess argon present.

Lavas from the Iran Tepe volcano, four km northeast of Ada Tepe give K–Ar ages of ~35 Ma but their stratigraphic position above the Upper Priabonian–Lower Oligocene marl-limestone formation suggests that they are younger than 34 Ma.

$^{40}Ar/^{39}Ar$ measurements on muscovite and biotite (Bonev et al., accepted) from the Gneiss-migmatite complex, record ages of 38.13 ± 0.36 and 37.73 ± 0.23 Ma, respectively (Table 1). These ages are broadly in agreement with the published $^{40}Ar/^{39}Ar$ ages for muscovite (42.2 ± 5.0 and 36.1 ± 5.0 Ma; Lips et al., 2000) and muscovite and amphibole (39 ± 1 and 45 ± 2 Ma, respectively; Mukasa et al., 2003) from the Biala Reka metamorphic core complex. Similar ages (39–35 Ma) have been obtained by Peytcheva et al. (1992) for the closing of Sr isotope system in the metagranites from the Biala Reka dome.

The relative age of the mineralization was determined based on its relationship with the host Krumovgrad group and the overlying Upper

Table 1 Summary of $^{40}Ar/^{39}Ar$ incremental heating experiments on adularia, sanidine, biotite and muscovite from Ada Tepe deposit and Kessebir dome.

Sample	Mineral	Weighted Plateau age (Ma)	Total Fusion age (Ma)	Source
AT01-2	adularia	34.99 ± 0.23	35.05 ± 0.23	this study
AT01-17	sanidine	31.82 ± 0.20	31.88 ± 0.20	this study
H6	biotite	37.73 ± 0.25	37.56 ± 0.24	Bonev et al. (accepted)
H706	muscovite	38.13 ± 0.36	38.34 ± 0.31	Bonev et al. (accepted)

Table 2 $^{40}Ar/^{39}Ar$ incremental-heating analyses of adularia and sanidine from Ada Tepe.

Experiment number	Laser power (Watts)	^{36}Ar (Volts)	± 1σ	^{37}Ar[a] (Volts)	± 1σ	^{38}Ar (Volts)	± 1σ	^{39}Ar[a] (Volts)	± 1σ	^{40}Ar (Volts)	± 1σ	^{40}Ar* (%)	^{39}Ar (%)	K/Ca	Age (Ma)[b]	± 2σ
AT01-2 adularia; J = 0.002987 ± 0.000009; mass discrimination per amu: 1.0022 ± 0.0004.																
AB2121	0.04 W	0.012604	0.000030	0.000159	0.000005	0.002772	0.000021	0.029850	0.000077	3.871564	0.001557	4.7	0.4	6.1	32.72	± 3.84
AB2122	0.10 W	0.009696	0.000022	0.004566	0.000046	0.004738	0.000020	0.239380	0.000131	4.348793	0.003120	34.9	2.9	1.6	33.85	± 0.38
AB2123	0.16 W	0.008804	0.000015	0.005107	0.000032	0.006792	0.000030	0.427709	0.000337	5.368227	0.002780	52.2	5.3	2.6	34.93	± 0.18
AB2124	0.22 W	0.003814	0.000011	0.000564	0.000010	0.003949	0.000012	0.268571	0.000112	2.865288	0.000789	61.3	3.3	15.0	34.83	± 0.16
AB2126	0.30 W	0.008692	0.000011	0.000261	0.000002	0.009565	0.000020	0.650692	0.000347	6.809601	0.002755	62.7	8.0	79.9	35.01	± 0.11
AB2127	0.45 W	0.011765	0.000015	0.000226	0.000006	0.017464	0.000035	1.258986	0.000312	11.697117	0.006487	70.5	24.8	177.0	35.00	± 0.09
AB2128	0.69 W	0.013209	0.000022	0.000199	0.000003	0.017401	0.000014	1.230663	0.001217	11.960795	0.012113	67.6	37.9	195.9	35.11	± 0.15
AB2129	1.25 W	0.012274	0.000021	0.000249	0.000003	0.017405	0.000037	1.255200	0.000803	11.896055	0.004493	69.8	17.3	161.1	35.32	± 0.10
											Plateau age				34.99	± 0.23
											MSWD (n = 5 of 8)				1.86	
											Total Fusion Age				35.05	± 0.23
AT01-17a sanidine; J = 0.002976 ± 0.000009; mass discrimination per amu: 1.0022 ± 0.0004.																
AB2132	0.04 W	0.000551	0.000005	0.000014	0.000006	0.000175	0.000005	0.003621	0.000024	0.182522	0.000076	11.8	0.0	45.6	31.31	± 4.56
AB2133	0.06 W	0.000193	0.000004	0.000026	0.000003	0.000343	0.000006	0.025791	0.000046	0.214316	0.000110	74.5	0.3	44.7	32.60	± 0.51
AB2134	0.12 W	0.000188	0.000004	0.000116	0.000007	0.002511	0.000023	0.204688	0.000253	1.288211	0.000967	95.9	2.0	56.8	32.08	± 0.12
AB2136	0.18 W	0.000503	0.000004	0.000568	0.000012	0.015207	0.000032	1.251793	0.000404	7.625113	0.002510	98.0	12.4	67.8	31.81	± 0.04
AB2137	0.24 W	0.000560	0.000005	0.000843	0.000018	0.023512	0.000025	1.921939	0.000651	11.637885	0.004597	98.5	19.0	70.0	31.79	± 0.04
AB2138	0.27 W	0.000361	0.000008	0.000707	0.000010	0.019152	0.000024	1.578728	0.000654	9.556079	0.004091	98.8	15.6	68.6	31.87	± 0.05
AB2139	0.31 W	0.000363	0.000001	0.000522	0.000008	0.014727	0.000035	1.202936	0.000478	7.300394	0.003784	98.5	11.9	70.9	31.84	± 0.05
AB2141	0.35 W	0.000311	0.000007	0.000377	0.000008	0.010541	0.000029	0.878996	0.000319	5.353642	0.002077	98.3	8.7	71.6	31.88	± 0.05
AB2142	0.45 W	0.000328	0.000004	0.000553	0.000015	0.015927	0.000034	1.307859	0.000548	7.947037	0.003239	98.7	12.9	72.6	31.96	± 0.05
AB2143	0.59 W	0.000285	0.000005	0.000394	0.000012	0.010851	0.000045	0.891613	0.000557	5.430367	0.002402	98.4	8.8	69.6	31.93	± 0.06
AB2145	0.84 W	0.000160	0.000004	0.000196	0.000007	0.005603	0.000028	0.451835	0.000332	2.760099	0.001984	98.3	4.5	70.6	31.97	± 0.08
AB2146	1.35 W	0.000166	0.000005	0.000183	0.000004	0.004620	0.000018	0.382947	0.000252	2.353853	0.001397	98.0	3.8	64.7	32.05	± 0.08
											Plateau age			31.82	± 0.20	
											MSWD (4 of 12)				2.79	
											Total Fusion Age				31.88	± 0.20

[a] Corrected for ^{37}Ar and ^{39}Ar decay

[b] Ages calculated relative to 28.34 Ma Taylor Creek Rhyolite standard; italics indicate steps omitted from the plateau age calculation, see text for details.

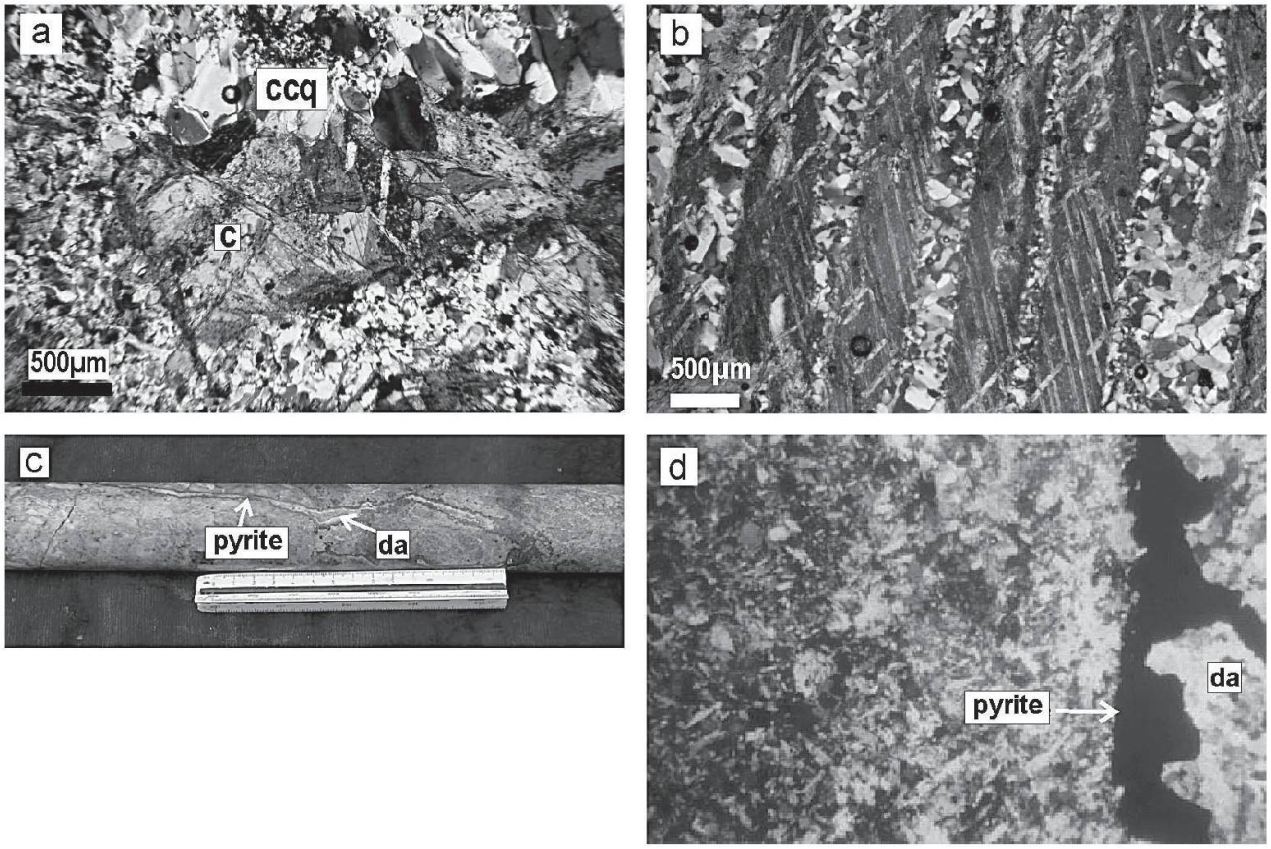

Fig. 7 (a) Geode of coarse-crystalline quartz with carbonate infill (third stage). (b) Third stage coarse-crystalline quartz (ccq) and bladed parallel type calcite (c). (c) Late vein (forth stage) composed by pyrite on its margins followed by dolomite-ankerite (da). (d) Same fracture. Dolomite-ankerite forms a halo overlapping quartz-adularia-pyrite alteration

Eocene–Oligocene sedimentary rocks. The latter is represented by sandstones unaffected by hydrothermal alteration, which cover the northern part of the deposit.

8. Sr and Pb isotope compositions of carbonates and pyrite

Sr and Pb isotopes were measured by standard TIMS procedures at the University of Geneva, Switzerland, following the methods of Valenza et al. (2000) and Chiaradia and Fontboté (2002). Sr isotope ratios on carbonate and Pb isotope ratios from pyrite at Ada Tepe along with whole rock Sr and Pb isotope ratios of the leachate fraction of a sample from Synap prospect, 2 km west of Ada Tepe, are presented in Table 3 and Figs. 9 and 10. The Ada Tepe carbonate is from a late stage ankerite-dolomite vein, taken from a drill-core sample (AT01-22) at 99.6 m depth. The bulk rock (sample Sin2000-28) from Synap is from sericite-adularia alteration from the surface. Pyrite from Ada Tepe is from a strongly silicified sample (Km2000-6). Pyrite from Synap is from the same hand sample Sin2000-28 on which the Sr was measured. Both samples belong to the early alteration. The initial $^{87}Sr/^{86}Sr$ ratio of the whole rock, corrected for 35 Ma, is 0.70809. The pyrite sample and whole rock leachate show identical $^{207}Pb/^{204}Pb$ (15.68) and $^{208}Pb/^{204}Pb$ (38.85) ratios and slightly different $^{206}Pb/^{204}Pb$ ratios (18.71 in Ada Tepe and 18.66 in Synap). The Sr and Pb isotope data are compared with those of local Paleogene volcanic rocks and dykes and the Rhodope metamorphic rocks in Figs. 9 and 10.

9. Discussion

9.1. Physical environment

Epithermal quartz from the Ada Tepe deposit is poor in fluid inclusions, particularly the early microcrystalline quartz and opal. Euhedral late sugary quartz is the only phase which contains larger fluid inclusions, but with no reliable characteristics that may allow to classify them as primary inclusions. For the similar Sleeper deposit, U.S.A., Saunders (1994) suggested that quartz formed by transformation of poorly ordered silica may exclude trapped fluids, thus precluding the use of microthermometry to constrain the physicochemical conditions of silica and gold deposition.

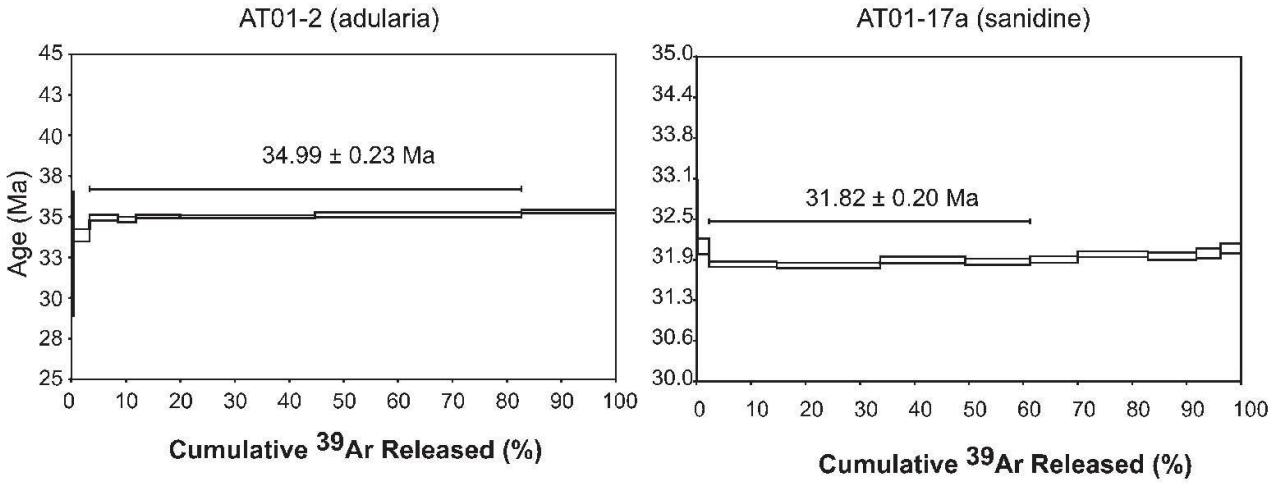

Fig. 8 $^{40}Ar/^{39}Ar$ incremental-heating age spectra for adularia from Ada Tepe and sanidine from rhyolite dyke from Kessebir dome.

The presence of adularia that spans the time of hydrothermal mineralization from the early microcrystalline stage to deposition of bonanza electrum bands accompanied by early bladed calcite and followed by late bladed Ca–Mg–Fe carbonates is consistent with boiling during most of the hydrothermal process (Izava et al., 1990; Simmons and Christenson, 1994). Evidence for boiling occurs throughout the Ada Tepe deposit from the present-day surface down to the detachment surface. The absence of bladed calcite in the veinlets beneath the detachment, however, suggests that boiling started as the fluid reached the sedimentary sequence. Boiling cools the fluid and concentrates dissolved silica, leading to precipitation of silica colloids (Saunders, 1994). Thus, much of the mineralization in The Wall appears to coincide with the onset of boiling.

Thermal conditions can be roughly evaluated on the basis of the distribution of temperature-sensitive minerals. The absence of epidote in the host-rock alteration can be interpreted in favor of a low-temperature (<240 °C) for the initial fluids (Bird et al., 1984; Rayes, 1990). This is confirmed by the large distribution of kaolinite, crystallizing at temperatures <200 °C (Simmons and Browne, 2000) and deposition of microcrystalline silica (chalcedony) or its transformation to jigsaw quartz in the stage of massive silicification, which occurs at temperature of >180 °C (Fournier, 1985). Thus, the temperature of the early fluid seems to have been 200–180 °C. Deposition of bonanza opal-electrum bands, however, requires considerably lower temperatures (100–150 °C; Hedenquist et al., 2000), suggesting a significant drop of temperature (see also Saunders, 1994). Such cooling can be attributed to simple boiling, causing cooling during decompression and increase in pH and fO_2 which accompanies the loss of dissolved gasses. Alternatively, it can be the result of mixing with cooler meteoric groundwater, in a manner similar to that described for the Hishikari low-sulfidation deposit (Izawa et al., 1990). Mixing of cool oxidized meteoric water with a hot, reduced deep crustal fluid has been proposed for low-angle faults bounding several metamorphic core complexes (Kerrich and Rehring, 1987; Kerrich and Hyndman, 1987; Spencer and Welty, 1986; Beaudoin et al., 1991).

9.2. Paleodepth

Mineralogical and textural characteristics, such as bladed carbonates and crustiform and colloform banded chalcedony and opaline silica plus adularia (Izawa et al., 1990; Cook and Simmons, 2000) suggest that the depth for the formation of mineralization at Ada Tepe deposit was shallow. In the absence of precise temperature and salinity data from fluid inclusion studies, the paleodepth of the Ada Tepe deposit cannot be precisely constrained. A minimum depth can be roughly estimated assuming boiling of low salinity solutions (<1 wt% NaCl equivalent) at a temperature of 200 °C. The depth of boiling of such a fluid below the water table is about 160–170 m (Haas, 1971).

Table 3 Sr and Pb isotope compositions of carbonate, pyrite and whole rock from Ada Tepe deposit and Synap mineralization.

Sample	AT 01-22 carbonate	Sin2000-28 bulk rock	KM 2000-6 pyrite
Rb		218	
Sr		82	
$^{87}Rb/^{86}Sr$		7.6950	
$^{87}Sr/^{86}Sr$	0.709270±14	0.711911±10	
$(^{87}Sr/^{86}Sr)_i$		0.70809	
$^{206}Pb/^{204}Pb$		18.663	18.707
$^{207}Pb/^{204}Pb$		15.682	15.684
$^{208}Pb/^{204}Pb$		38.849	38.843

For fluids under a hydrodynamic gradient and containing dissolved CO_2, the depth of boiling would be somewhat deeper (Hedenquist and Henley, 1985). This is consistent with the 350 m thickness of the host Shavarovo Formation (Goranov and Atanasov, 1992), which implies that the overlying coal-bearing-sandstone and marl-limestone formations had not yet been deposited when the ore formed.

9.3. Sources and relationships among mineralization, extension and magmatism

The new $^{40}Ar/^{39}Ar$ ages from adularia and sanidine have been compared with those from muscovite and biotite in the Kessebir dome (Bonev et al., accepted), K–Ar ages of nearby Iran Tepe volcano (Lilov et al., 1987) and intra-plate alkaline basalts (Marchev et al., 1997, 1998) to clarify relationships between volcanism, thermal events in the Kessebir dome and mineralization in the Ada Tepe deposit. As discussed above, the $^{40}Ar/^{39}Ar$ total fusion age of adularia (Marchev et al., 2003) shows that the mineralization at Ada Tepe formed at 35 Ma. Mineralization may have been coeval with 35 Ma lavas of the Iran Tepe paleovolcano (Lilov et al., 1987; Pecskay, pers. comm.), however, the uncertainties of the dating methods do not rule out differences in age on the order of several 100 kyr. Notwithstanding, field relationships indicate that volcanic activity of the Iran Tepe volcano is younger than the Krumovgrad group.

Another possible source of fluids and metals is the magmatism of the Kessebir dome itself. Comparison of the timing of Ada Tepe mineralization (35 Ma), the Kessebir rhyolite dyke (31.82 ± 0.20 Ma) and K–Ar ages of intra-plate alkaline basalts (28–26 Ma) show that mineralization preceded by at least 3 Ma the rhyolitic magmatism and at least 6 Ma the intra-plate basalts. Thus, it is highly unlikely that this younger igneous activity was the source of Ada Tepe mineralizing fluids or heat.

Mineralization at Ada Tepe is ca. 3 Ma younger than the $^{40}Ar/^{39}Ar$ ages of the muscovite (38.13 ± 0.36) and biotite (37.73 ± 0.25 Ma) from the lower plate of the Kessebir dome. Recently obtained older $^{40}Ar/^{39}Ar$ age for amphibole (45 ± 2 Ma) and similar age for the muscovite (39 ± 1 Ma) in the Biala Reka dome (Mukasa et al., 2003) have been interpreted as cooling ages for the upper plate. Therefore, muscovite and biotite ages from Kessebir can be interpreted as cooling of the lower plate rocks to below 350–300 °C following the Maastrichtian–Paleocene metamorphism (Marchev et al., 2004). The latter ages are generally consistent with a 42–35 Ma range of ages, obtained earlier by Peytcheva (1997) for the closing of Rb–Sr system in the granitoids in Biala Reka and Kessebir, after a presumable amphibolite facies metamorphism. Ore deposit formation at ~35 Ma in the hanging wall of the Tokachka detachment coincides with late stage brittle extension after cooling of the basement rocks at temperatures < 200 °C (Bonev et al., accepted). The highest grade portion of the ore mineralization (The Wall) is dominated by multiple phases of veining and brecciation suggesting a syndetachment evolution of the hydrothermal process. The presence of several unconformities in the overlying Upper Eocene–Lower Oligocene coal-bearing-sandstone and marl-limestone formations (Goranov and Atanassov, 1992; Boyanov and Goranov, 1994, 2001), suggests a continuation of the uplift and exhumation of the Kessebir dome even several million years after the formation of the Ada Tepe deposit.

Probable source rocks for the Sr (Ca) and Pb can be constrained by comparison of the Sr and Pb isotope ratios of carbonates and pyrites from Ada Tepe with the major source rocks (Figs. 9 and

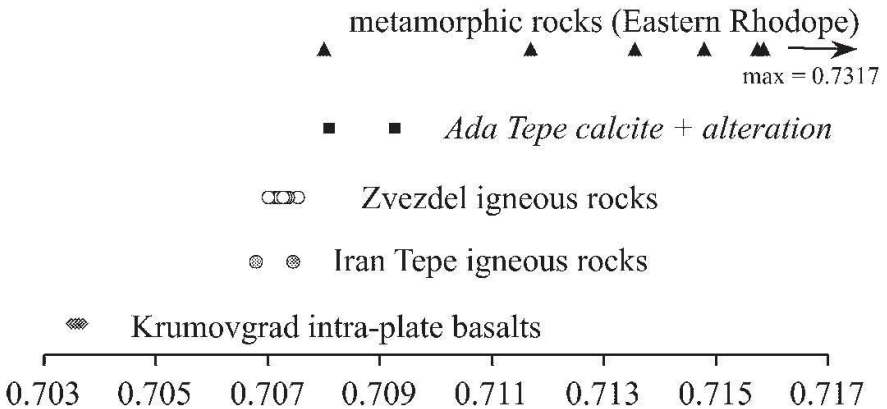

Fig. 9 Sr isotope composition of calcite from Ada Tepe and whole rock sample from Synap compared with Krumovgrad area igneous and metamorphic rocks. Data for the intra-plate basalts – Marchev et al., 1998; for the Zvezdel and Iran Tepe lavas – Marchev, unpublished data; for the metamorphic rocks – Peytcheva et al., 1992 and Pljusnin et al., 1988).

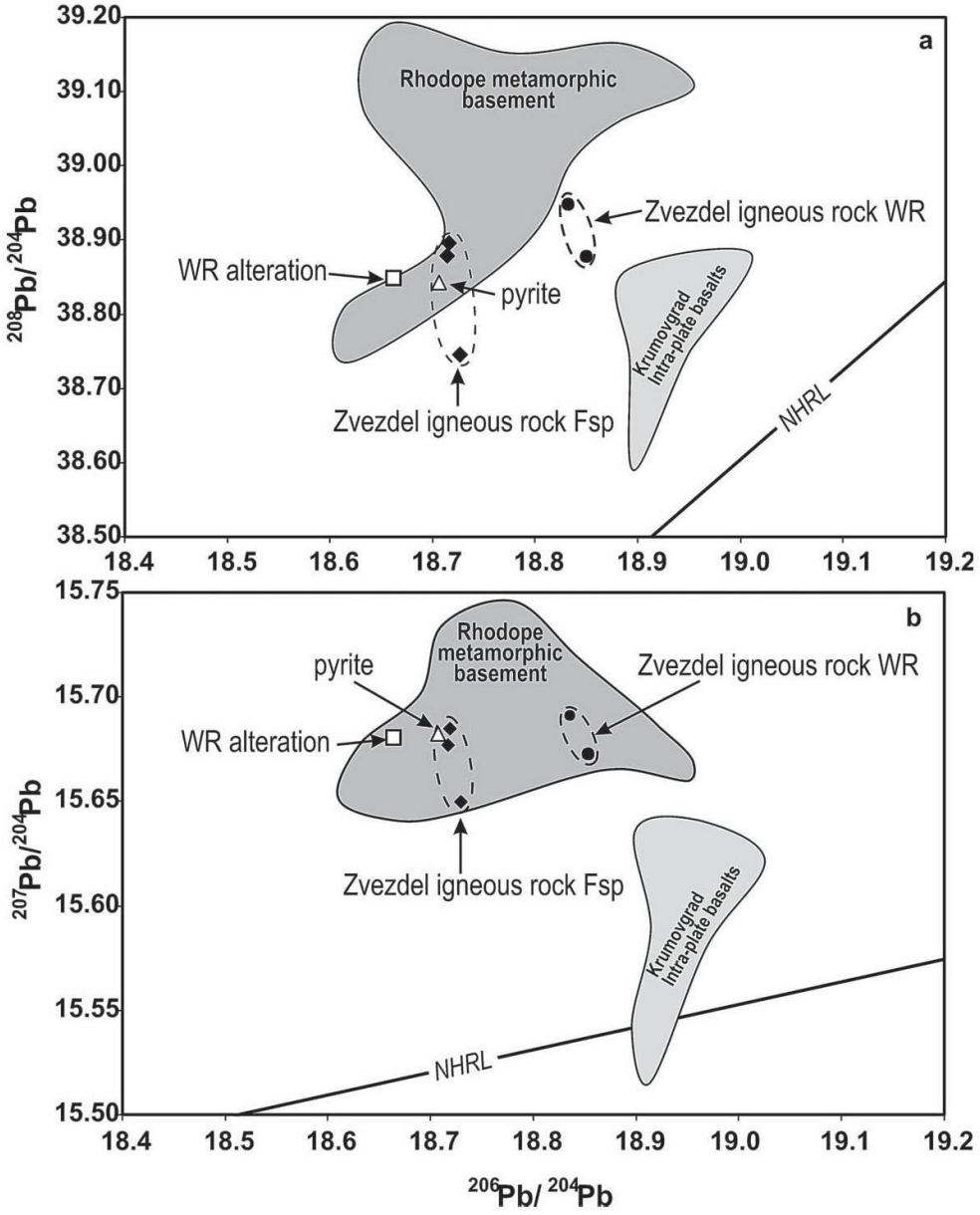

Fig. 10 Pb isotope composition of pyrite (Ada Tepe) and whole rock alteration (Synap), compared with feldspars and whole rocks from Zvezdel Oligocene volcano (Marchev et al., unpubl. data) and whole rocks from Krumovgrad intra-plate basalts (Marchev et al. (1998) and Rhodope metamorphic rocks from Frei (1995).

10). Bulk rock and carbonate Sr isotope data (0.70809–0.70927), lie within the lower range of present-day $^{87}Sr/^{86}Sr$ isotopic ratios between 0.708–0.737 for the prevailing gneissic metamorphic rock within the Eastern Rhodopes (Peytcheva et al., 1992) and are higher than the Sr isotopic values of the nearby younger igneous rocks from Iran Tepe and Zvezdel volcanoes (0.70641–0.70741; Marchev et al., unpubl. data). It appears likely that the hydrothermal Sr and, by inference Ca, is mostly of metamorphic origin or represent a mixture of metamorphic and small amount of old magmatic source isotopically similar to Iran Tepe and Zvezdel magmas (see below).

Pyrite Pb isotope ratios overlap with the field of feldspars from Zvezdel igneous rocks, however, the leachate fraction of the whole rock sample from Synap has a slightly lower $^{206}Pb/^{204}Pb$ ratio than the feldspars. Collectively, the two samples plot in the fields of the Rhodope metamorphic rocks. From these data, it is not possible to discriminate between a metamorphic and an igneous origin of Pb in the hydrothermal fluid. This is not surprising as orogenic igneous rocks of the Eastern Rhodopes were strongly contaminated with crustal Pb (Marchev et al. 1998 and 2004) and differ isotopically from the asthenospheric-derived Krumovgrad intra-plate basalts (Fig. 10). Therefore, isotopic homogenization of the orogenic igneous and metamorphic rocks in the region limits the possibility to discriminate between these two sources. Nevertheless, it may be suggested that fluid circulation through the metamorphic basement rocks and metamorphic-derived sediments

would cause a large contribution from metamorphic lead.

Thus, the simplest genetic model to explain the geology, geochronology, and Sr and Pb isotopes involves hydrothermal convection through the Paleozoic metamorphic basement. The close temporal association of mineralization at Ada Tepe with the exhumation processes and formation of the Kessebir dome favours a genetic link between them. We propose that the metamorphic basement rocks provided the heat to drive the hydrothermal system. During exhumation, however, the lower plate of the Kessebir metamorphic core complex experienced cooling and decompression since the Upper Cretaceous (Marchev et al., 2004). This has been used in other metamorphic complexes (Smith et al., 1991) to argue that prograde metamorphic devolatilization of the lower plate is unlikely to generate fluid responsible for mineralization during extension. These authors suggested that igneous rather than metamorphic fluid source is more likely for the metamorphic core complex-related mineralization. This apparent contradiction can be explained by asthenospheric upwelling that was operating in the Eastern Rhodope area (Marchev et al., 2004) causing retrograde metamorphism at shallow levels and at the same time resulting in prograde metamorphism at deeper levels observed by the high heat flow in the region. Although magmatic activity seems to be younger than the ore mineralization, the first erupted lavas of Iran Tepe were close in time. The beginning of this volcanism was probably preceded by accumulation of magma at greater depths. Under such conditions, fluids liberated by deep prograde devolatilization reactions and/or mantle degassing could ascend to form low temperature fluids.

9.4. Gold deposits associated with detachment faults

Different types of mineralization in low-angle detachment faults associated with metamorphic core complexes are described mostly in the southwestern United States. These include Picacho, (Drobeck et al., 1986; Liebler, 1988) and Bullard Peak (Roddy et al., 1988), Southwestern Arizona; and Riverside Pass (Wilkinson et al., 1988) and Whipple-Buckskin-Rawhide (Spencer and Welty, 1986), Southeastern California. Another example is in the Kokanee Range, Southern British Columbia, Canada (Beaudoin et al., 1991).

These kinds of deposits are divided by Eng et al. (1988) into two categories: base-metal enriched (Whipple-Buckskin-Rawhide and Kokanee deposits) and base-metal poor (Picacho and Riverside Pass). In the base-metal poor deposits gold is typically associated with silicification and hematite (Picacho), or hematite and chrisocolla (Riverside Pass). Pyrite, which is entirely oxidized in Riverside Pass, is the principal sulfide mineral. Quartz and lesser calcite are the main gangue minerals

Mineralization at Ada Tepe deposit shares many characteristics with Picacho and Riverside Pass, including association of gold with multiple episodes of silicification and veining within shallowly dipping detachment faults, and a low content of base-metals and As. However, comparison of the characteristics of Ada Tepe to other base-metal poor detachment-related mineralizations reveals several notable differences. These include lack of copper and specular hematite, a relatively high content of adularia and various silica polymorphs and carbonates. These features may reflect differences in crustal compositions and history, the nature of the ore-forming hydrothermal fluids, and physico-chemical conditions at the focus of ore deposition.

10. Conclusions

(1) Based on alteration, mineralization and textures, we classify Ada Tepe as a low-sulfidation epithermal gold deposit, hosted in sedimentary rocks.

(2) The Tokachka low-angle detachment fault and the steep listric faults in the Maastrichtian-Paleocene sedimentary sequence were the major sites of gold mineralization. There are many indicators, including breccias, that synmineralization movement took place along the detachment surface.

(3) The deposit formed at shallow depth, less than 200–250 m below the paleosurface. Microcrystalline quartz and opal, which are the main silica polymorphs crystallizing with the electrum bands, preclude the use of fluid inclusion to constrain the conditions of gold deposition. From other alteration minerals temperature of formation is evaluated to <200 °C. The mineralogy suggests that the fluid boiled throughout the deposit.

(4) Mineralization is an exclusively Au system with traces of As and with no base metals. The majority of the gold occurs as electrum with 73–76% Au, which is reflected in the average Au/Ag ratio (~3) of the deposit.

(5) The $^{40}Ar/^{39}Ar$ age of adularia indicates that the ore was deposited at Ada Tepe at 35.0 ± 0.2 Ma. This age is ~3 Ma younger than the closure of metamorphic muscovite and biotite at ~350 °C in the underlying basement, and 3 Ma older than sa-

nidine in the nearest rhyolite, thereby precluding local magmatism as a source of fluids or heat.

(6) Sr and Pb isotope ratios are consistent with the idea that metals and carbonates were probably derived from the metamorphic basement rocks with a possible contribution from an igneous source.

(7) Collectively, these data suggest an intimate association of Ada Tepe Au mineralization to the metamorphic core-complex formation rather than to the local magmatism.

Acknowledgments

This is a contribution to the ABCD-GEODE program of the European Science Foundation. Supported by the Swiss National Science Foundation Joint Research Project 7BUPJ062276 and grants 21-59041.99 and 200020-101853. $^{40}Ar/^{39}Ar$ analyses at UW-Madison supported by US NSF grants EAR-10114055 and EAR-0337667 to Singer. BMM gave permission to publish these results and provided financial support. The authors appreciate the comments and helpful reviews of the journal reviewers D. Altherton, N. Skarpelis and Albrecht von Quadt. Denis Fontignie and Massimo Chiaradia (Universities of Geneva, Switzerland and Leeds, U.K.) are thanked for the Sr and Pb isotope analyses. Thanks are owed to Albrecht von Quadt and Ivan Bonev for etching of gold samples and the SEM pictures of the etched samples, respectively.

References

Atanasov, G. and Goranov, A. (1984): On the Palaeogeography of the East Rhodopes. *C. R. Acad. bulg. Sci.*, **37(6)**, 783–784.

Beaudoin, G., Taylor, B.E. and Sangster, D.F. (1991): Silver-lead-zinc veins, metamorphic core complexes, and hydraulic regimes during crustal extension. *Geology*, **19**, 1217–1220.

Belmustakova, H., Boyanov, I., Ivanov, I. and Lilov, P. (1995): Granitoid bodies in the Byala Reka dome. *C. R. Acad. bulg. Sci.*, **48** (4), 37–40 (in Russian).

Bird, D.K., Schiffman, P., Elders, W.A., Williams, A.E. and McDowell, S.D. (1984): Calc-silicate mineralization in active geothermal systems. *Econ. Geol.*, **79**, 671–695.

Bonev, N. (1996): Tokachka shear zone southwest of Krumovgrad in Eastern Rhodopes, Bulgaria: an extensional detachment. *Ann. Univ. Sofia*, **89**, 97–106.

Bonev, N. (2002): Structure and evolution of the Kessebir gneiss dome, Eastern Rodopes. PhD. thesis, Univ. of Sofia, unpubl., 282 pp. (in Bulgarian).

Bonev, N., Marchev, P. and Singer, B. (accepted): Interference between tectonic, ore-forming and magmatic processes during the Tertiary extensional exhumation in the Eastern Rhodope (Bulgaria): $^{40}Ar/^{39}Ar$ geochronology constraints. *Geodin. Acta*.

Boyanov, I. and Goranov, A. (1994): Paleocene–Eocene sediments from the Northern periphery of the Borovica depression and their correlation with similar sediments in the East Rhodopean Paleogene depression. *Rev. Bulg. Geol. Soc.*, **55(1)**, 83–102 (in Bulgarian with English abstract).

Boyanov, I. and Goranov, A. (2001): Late Alpine (Paleogene) superimposed depressions in parts of Southeast Bulgaria. *Geol. Balc.*, **34(3–4)**, 3–36.

Carrigan, C., Mukasa, S., Haydoutov, I. and Kolcheva, K. (2003): Ion microprobe U–Pb zircon ages of pre-Alpine rocks in the Balkan, Sredna Gora, and Rhodope terranes of Bulgaria: Constraints on Neoproterozoic and Variscan tectonic evolution. *J. Czech Geol. Soc.* Abstract volume **48/1–2**, 32–33.

Chiaradia, M. and Fontboté, L. (2002): Separate lead isotope analyses of leachate and residue rock fractions: implications for metal source tracing in ore deposit studies. *Mineral. Deposita*, **38**, 185–195.

Cook, D.R and Simmons, S.F. (2000): Characteristics and genesis of epithermal gold deposits. *Reviews Econ. Geol.*, **13**, 221–224.

Crummy, J. (2002): A speculative genetic model for the location of gold mineralization on the Krumovgrad license, SE Rhodope, Bulgaria. *Geol. Mineral. Res.*, **1**, 20–24.

Duffield, W. and Dalrymple, G.B. (1990): The Taylor Creek Rhyolite of New Mexico: a rapidly emplaced field of lava domes and flows. *Bull. Volcanol.*, **52**, 475–487.

Drobeck, P.A., Hillemeyer, J.L., Frost, E.G and Liebler, G.S. (1986): The Picacho Mine: a gold mineralized detachment in southeastern California. In: Beatty, B. and Wilkinson, P.A.K. (eds): Frontiers in geology and ore deposits of Arizona and the Southwest. *Arizona Geol. Soc. Digest.* **XVI**, Tucson, 187–221.

Eng, T., Boden D.R., Reischman, M.R. and Biggs, J.O. (1995): Geology and mineralization of the Bullfrog Mine and vicinity, Nye County, Nevada. In: Coyner, A.R. and Fahey, P.L. (eds.): Geology and ore deposits of the American Cordillera. Symposium Proceedings, Geol. Soc. Nevada, Reno/Sparks, Nevada. **Vol.1**, 353–400.

Fournier, R.O. (1985): Silica minerals as indicators of conditions during gold deposition: *U.S. Geol. Survey Bull.* **1646**, 15–26.

Frei, R. (1995): Evolution of mineralizing fluid in the porphyry copper system of the Scouries deposit, Northeast Chalkidiki (Greece): Evidence from combined Pb–Sr and stable isotope data. *Econ. Geol.*, **90**, 746–762.

Goranov, A. and Atanasov, G. (1992): Lithostratigraphy and formation conditions of Maastrichtian-Paleocene deposit in Krumovgrad District. *Geol. Balc.*, **22(3)**, 71–82.

Haas, J.L. Jr. (1971): The effect of salinity on the maximum thermal gradient of a hydrothermal system at hydrostatic pressure. *Econ. Geol.*, **66**, 940–946.

Hedenquist, J.W. and Henley, R.W. (1985): The importance of CO_2 on freezing point measurment of fluid inclusions: evidence from active geothermal systems and implications for epithermal ore deposition. *Econ. Geol.*, **80**, 1379–1399.

Hedenquist, J.W. Arribas, A.R. and Gonzales-Urien, E. (2000): Exploration for epithermal gold deposits. *Soc. Econ. Geol. Reviews*, **13**, 245–277.

Izawa, E., Urashima, Y., Ibaraki, K., Suzuki, R., Yokoyama, T., Kawasaki, K., Koga, A. and Taguchi, S. (1990): The Hishikari gold deposit: High grade epithermal veins in Quaternary volcanics of southern Kyushu, Japan. *J. Geochem. Explor.*, **36**, 1–56.

Kerrich, R. and Rehring, W. (1987): Fluid motion associated with Tertiary mylonitization and detachment faulting: $^{18}O/^{16}O$ evidence from the Picacho metamorphic core complex, Arizona. *Geology*, **15**, 58–62.

Kerrich, R. and Hyndman, D. (1987): Thermal and fluid regimes in the Bitteroot lobe-Sapphire block detachment zone, Montana: Evidence from $^{18}O/^{16}O$ and geologic relations. *Geol. Soc. Am. Bull.*, **97**, 147–155.

Kolcheva, K. and Eskenazy, G. (1988): Geochemistry of metaeclogites from the Central and Eastern Rhodope Mts (Bulgaria). *Geol. Balc.*, **18**, 61–78.

Kozhoukharov, D., Kozhoukharova, E. and Papanikolaou, D. (1988): Precambrian in the Rhodope massif. In: Zoubek, V. (ed.): Precambrian in Younger Fold Belts, Chichester, 723–778.

Kozhoukharova, E. (1984): Origin and structural position of the serpentinized ultrabasic rocks of the Precambrian ophiolitic association in the Rhodope Massif. I: Geologic position and composition of ophiolite association. *Geol. Balc.*, **14**, 9–36 (in Russian).

Kunov, A., Stamatova, V., Atanasova, R. and Petrova, P. (2001): The Ada Tepe Au-Ag-polymetallic occurrence of low-sulfidation (adularia-sericite) type in Krumovgrad district. *Mining and Geol.*, **2001(4)**, 16–20 (in Bulgarian).

Liebler, G.S. (1988): Geology and gold mineralization at the Picacho mine, Imperial County, California. In: Schafer, R.W., Cooper, J.J. and Vikre P.G. (eds): Bulk mineable precious metal deposits of the Western United States, Symposium Proceedings, Geol. Soc. Nevada, Reno/Sparks, Nevada. Part IV, Gold-silver deposits associated with detachment faults. 453–504.

Lilov, P., Yanev, Y. and Marchev, P. (1987): K/Ar dating of the Eastern Rhodopes Paleogene magmatism. *Geol. Balc.*, **17(6)**, 49–58.

Lips, A.L.W., White, S.H. and Wijbrans, J.R. (2000): Middle-Late Alpine thermotectonic evolution of the southern Rhodope Massif, Greece. *Geodin. Acta*, **13**, 281–292.

Marchev, P., Harkovska, A., Pecskay, Z., Vaselli, O. and Downes, H. (1997): Nature and age of the alkaline basaltic magmatism south-east of Krumovgrad, SE-Bulgaria. *C. R. Acad. bulg. Sci.*, **50(4)**, 77–80.

Marchev, P., Vaselli, O., Downes, H., Pinarelli, L., Ingram, G., Rogers, G. and Raicheva, R. (1998): Petrology and geochemistry of alkaline basalts and lamprophyres: implications for the chemical composition of the upper mantle beneath the Eastern Rhodopes (Bulgaria). In: Christofides, G., Marchev, P. and Serri, G. (eds.): Tertiary magmatism of the Rhodopian region. *Acta Vulcanologica*, **10/2**, 233–242.

Marchev, P. and Singer, B. (2002): $^{40}Ar/^{39}Ar$ geochronology of magmatism and hydrothermal activity of the Madjarovo base-precious metal ore district, eastern Rhodopes, Bulgaria. In: Blundell, D., Neubauer, F. and von Quadt, A. (eds.): The timing and location of major ore deposits in an evolving orogen. *Geol. Soc. London Spec. Publ.*, **204**, 137–150.

Marchev, P., Singer, B., Andrew, C., Hasson, A., Moritz, R. and Bonev, N. (2003): Characteristics and preliminary $^{40}Ar/^{39}Ar$ and $^{87}Sr/^{86}Sr$ data of the Upper Eocene sedimentary-hosted low-sulfidation gold deposits Ada Tepe and Rosino, SE Bulgaria: possible relation with core complex formation. In: Eliopoulos et al. (eds.): Mineral Exploration and Sustainable Development. Millpress, Rotterdam, 1193–1196.

Marchev, P., Raicheva, R., Downes, H., Vaselli, O., Massimo, C. and Moritz, R. (2004): Compositional diversity of Eocene-Oligocene basaltic magmatism in the Eastern Rhodopes, SE Bulgaria: implications for its genesis and geological setting. *Tectonophysics*, **393**, 301–328.

Marchev, P., Raicheva, R., Singer, B., Downes, H., Amov, B. and Moritz, R. (2000): Isotopic evidence for the origin of Paleogene magmatism and epithermal ore deposits of the Rhodope Massif. In: Geodynamics and Ore Deposit Evolution of the Alpine-Balkan-Carpathian-Dinaride-Province. Borovets, Abstracts ABCD-GEODE 2000 workshop Borovets, Bulgaria, p. 47.

Mposkos, E. and Krohe, A. (2000): Petrological and structural evolution of continental high pressure (HP) metamorphic rocks in the Alpine Rhodope Domain (N. Greece). In: Panayides, I., Xenopontos, C. and Malpas, J. (eds.): Proceedings of the 3rd International Conf. on the Geology of the Eastern Mediterranean (Nicosia, Cyprus). Geol. Survey, Nicosia, Cyprus, 221–232.

Mposkos, E. and Wawrzenitz, N. (1995): Metapegmatites and pegmatites bracketing the time of high P metamorphism in polymetamorphic rocks of the E-Rhodope, N. Greece: Petrological and geochronological constraints. *Geol. Soc. Greece Spec. Publ.*, **4(2)**, 602–608.

Mukasa, S., Haydoutov, I., Carrigan, C. and Kolcheva, K. (2003): Thermobarometry and $^{40}Ar/^{39}Ar$ ages of eclogitic and gneissic rocks in the Sredna Gora and Rhodope terranes of Bulgaria. *J. Czech Geol. Soc.* Abstract volume **48/1–2**, 94–95.

Ovtcharova, M., Quadt, A. von, Heinrich, C.A., Frank, M. and Kaiser-Rohrmeier, M. (2003). Triggering of hydrothermal ore mineralization in the Central Rhodopean Core Complex (Bulgaria) – Insight from isotope and geochronological studies on Tertiary magmatism and migmatization. In: Eliopoulos et al. (eds.): Mineral Exploration and Sustainable Development. Millpress, Rotterdam, 367–370

Peytcheva, I. (1997): The Alpine metamorphism in Eastern Rhodopes – Rb–Sr isotope data. *Rev. Bulg. Geol. Soc.*, **58(3)**, 157–165 (in Bulgarian with English abstract).

Peytcheva, I., Kostitsin, Y., Salnikova, E., Ovtcharova, M. and von Quadt, A. (1999): The Variscan orogen in Bulgaria – new isotope-geochemical data. *Rom. Jour. tectonics and regional geology*, **77**, Abstract volume, p. 72.

Peytcheva, I., Kostitsin, J.A. and Shukolyukov, J.A. (1992): Rb–Sr isotope system of gneisses in the South-Eastern Rhodopes (Bulgaria). *C. R. Acad. bulg. Sci.*, **45(10)**, 65–68 (in Russian).

Peytcheva, I., Ovcharova, M., Sarov, S. and Kostitsin, Y. (1998): Age and metamorphic evolution of metagranites from Kessebir reka region, Eastern Rhodopes – Rb–Sr isotope data. Abstracts XVI Congress CBGA, Austria, Vienna.

Peytcheva, I. and von Quadt, A. (1995): U–Pb dating of metagranites from Byala-Reka region in the East Rhodopes, Bulgaria. *Geol. Soc. Greece Spec. Publ.*, **4(2)**, 637–642.

Plyusnin, G.S., Marchev, P.G. and Antipin, V.S. (1988): Rubidium-Strontium age and genesis of the shoshonite-latite series in the Eastern-Rhodope, Bulgaria. *Dokl. Akad. Nauk SSSR*, **303(3)**, 719–724.

Reyes, A.G. (1990): Petrology of Philippine geothermal systems and the application of alteration mineralogy to their assessment. *J. Volcanol. Geotherm. Res.*, **43**, 279–309.

Ricou, L.E., Burg, J.P., Godfriaux, I. and Ivanov, Z. (1998): Rhodope and Vardar: the metamorphic and the olistostromic paired belts related to the Cretaceous subduction under Europe. *Geodin. Acta*, **11**, 285–309.

Roddy, M.S., Reynolds, S.J., Smith, B.M. and Ruiz, J. (1988): K metasomatism and detachment-related mineralization, Harcuvar Mountains, Arizona. *Geol. Soc. Am. Bull.*, **100**, 1627–1639.

Rohrmeier, M., Quadt, A.von, Handler, R., Ovtcharova, M., Ivanov, Z. and Heinrich, C. (2002): The geodynamic evolution of hydrothermal vein deposits in the Madan metamorphic core complex, Bulgaria. *Geochim. Cosmochim. Acta*, Special Supplement,

Abstracts of the 12th Ann. Goldschmidt Conference, Davos, Switzerland, 66, S1, A645.

Sarov, S. and twelve others (1996): Report for the results of execution of the geological task "Geological mapping in scale 1:25 000 and geomorphologic mapping in scale 1:50 000 with complex prognostic evaluation of the mineral resources in the area of Krumovgrad and villages Gornoseltsi, Popsko, Djanka and Nanovitsa (Eastern Rhodopes), on area of 485 km^2 National geofond, IV-438.

Saunders, J.A. (1990): Colloidal transport of gold and silica in epithermal precious-metal systems: Evidence from the Sleeper deposit, Nevada. *Geology*, **18**, 757–760.

Shabatov, Y. and eight others (1965): Report for the geological mapping, accompanied with prospecting for ore mineralizations in scale 1:25 000 in 1963–1964 in part of the SE Rhodopes. Geofond of Committee of Geology, IV-217.

Saunders, J.A. (1994): Silica and gold texture in bonanza ores of the Sleeper deposit, Humbolt county, Nevada: Evidence for colloids and implications for epithermal ore-forming processes. *Econ. Geol.*, **89**, 628–638.

Simmons, S.F. and Browne, P.R.L. (2000): Hydrothermal minerals and precious metals in the Broadlands-Ohaaki geothermal system: Implications for understanding low-sulfidation epithermal environments. *Econ. Geol.*, **95**, 971–999.

Simmons, S.F. and Christenson, B.W. (1994): Origins of calcite in a boiling geothermal system. *Am. J. Sci.*, **294**, 361–400.

Singer, B. and Brown, L.L. (2002): The Santa Rosa Event: $^{40}Ar/^{39}Ar$ and paleomagnetic results from the Vales rhyolite near Jaramillo Creek, Jemez Mountains, New Mexico. *Earth Planet. Sci. Lett.*, **197**, 51–64.

Singer, B. and Marchev, P. (2000): Temporal evolution of arc magmatism and hydrothermal activity, including epithermal gold veins, Borovitsa caldera, southern Bulgaria. *Econ. Geol.*, **95**, 1155–1164.

Smith, B.M., Reynolds, S.J., Day, H.W. and Bodnar, R.J. (1991): Deep-seated fluid involvement in ductile-brittle deformation and mineralization, South Mountain metamorphic core complex, Arizona. *Geol. Soc. Am. Bull.*, **103**, 559–569.

Spencer, J.E. and Welty, J.W. (1986): Possible controls of base- and precious-metal mineralization associated with Tertiary detachment faults in the lower Colorado River trough, Arizona and California. *Geology*, **14**, 195–198.

Stoyanov, R. (1979): Metallogeny of the Rhodope Central Massif. Nedra, Moscow, 180 pp. (in Russian).

Valenza, K., Moritz, R., Mouttaqi, A., Fontignie, D. and Sharp, Z. (2000): Vein and karstic barite deposits in the Western Jebilet of Morocco: Fluid inclusion and isotope (S,O,Sr) evidence for regional fluid mixing related to Central Atlantic rifting. *Econ. Geol.*, **95**, 587–605.

Wilkinson, W.H., Wendt, C.J. and Dennis, M.D. (1988): Gold mineralization along Riverside Mountains Detachment Fault, Riverside County, California. In: Schafer, R.W., Cooper, J.J. and Vikre P.G. (eds.): Bulk mineable precious metal deposits of the Western United States, Symposium Proceedings, Geol. Soc. Nevada, Reno/Sparks, Nevada. Part IV, Gold-silver deposits associated with detachment faults, 487–504.

Received 24 March 2003
Accepted in revised form 23 July 2004
Editorial handling: A. von Quadt